Gas-phase kinetic measuremets and quantum chemical calculations of the ligation of Ni+, Cu+, Ni+(pyrrole)1,2 and Cu+(pyrrole)1,2 with O2 and CO

ARTICLE *in* INTERNATIONAL JOURNAL OF MASS SPECTROMETRY · MAY 2003

Impact Factor: 1.97 · DOI: 10.1016/S1387-3806(03)00046-0

Available online at www.sciencedirect.com
SCIENCE DIRECT®
International Journal of Mass Spectrometry 227 (2003) 161–173
International Journal of Mass Spectrometry
www.elsevier.com/locate/ijms

Gas-phase kinetic measurements and quantum chemical calculations of the ligation of Ni^+, Cu^+, $Ni^+(pyrrole)_{1,2}$ and $Cu^+(pyrrole)_{1,2}$ with O_2 and CO

Michael J.Y. Jarvis, Luca F. Pisterzi, Voislav Blagojevic, Gregory K. Koyanagi, Diethard K. Bohme*

Department of Chemistry, Centre for Research in Mass Spectrometry and Centre for Research in Earth and Space Science, York University, Toronto, Ont., Canada M3J 1P3

Received 16 October 2002; accepted 6 January 2003

Dedicated to Robert Dunbar on the occasion of his 60th birthday and in recognition of his many valuable contributions to gas-phase ion chemistry.

Abstract

The rate and equilibrium kinetics of the reactions of M^+, M^+(pyrrole) and $M^+(pyrrole)_2$ (M = Ni, Cu) with the small diatomic ligands O_2 and CO have been investigated in the gas phase at 295 ± 2 K in helium buffer gas at a pressure of 0.35 ± 0.01 Torr. The measurements were taken with an inductively-coupled plasma/selected-ion flow tube (ICP-SIFT) tandem mass spectrometer. Only ligation was observed. While atomic Cu^+ was observed to bind up to two ligands of O_2 and CO, atomic Ni^+ was observed to bind up to three. The presence of one molecule of pyrrole dramatically increases the gas-phase rate of metal-ion ligation except for the ligation of Cu^+ with O_2. $Ni^+(pyrrole)_2$ and $Cu^+(pyrrole)_2$ were found to be unreactive with O_2, $k < 1.0 \times 10^{-13}$ cm^3 molecule^{-1} s^{-1}, but both ions were observed to ligate a single molecule of CO. While equilibrium was observed to be approached in several of the ligation reactions, an absolute value for the standard free energy of ligation could be obtained only for the ligation of Ni^+(pyrrole)(CO) with CO. Quantum chemical calculations using density functional theory (DFT) with the B3LYP (Becke-3 Lee–Yang–Parr) hybrid functional have provided insight into the energetics and geometries of ligation. The bonding of pyrrole to either Ni^+ or Cu^+ is much stronger than bonding of either O_2 or CO. This agrees with the failure to observe experimentally any ligand-switching reactions involving the pyrrole ligand. Also, the computations show that the ligation of pyrrole does not significantly change the ligation energy of O_2 and CO to the metal ions. The various isomers of CO-containing complexes were investigated and it was found that metal–C bonding was always thermodynamically favored over metal–O bonding. The computations also show that the addition of a ligand of O_2 or CO can skew the symmetry inherent in M^+–pyrrole complexes (but less so with O_2) by shifting the position of the metal ion relative to the midline of the pyrrole molecule. The structures determined for the various metal ion–CO complexes were found to have a linear M–CO geometry, while structures of metal ion–O_2 complexes were found to have a bent M–O_2 geometry.

Keywords: Ni^+; Cu^+; Pyrrole; CO; O_2; Ligation; ICP-SIFT

* Corresponding author. Tel.: +1-416-7362100x66188; fax: +1-416-736-5936.
E-mail address: dkbohme@yorku.ca (D.K. Bohme).

1387-3806/03/$ – see front matter
doi:10.1016/S1387-3806(03)00046-0

1. Introduction

Non-covalent inter- and intra-molecular interactions can be crucial in determining both structures and reactivites of bioorganometallic systems [1–4]. One of the most important of these is the strong attraction between metal cations and the π-face of aromatic molecules, of which benzene is a simple and common example [5–7]. In the larger context, it has been shown that metal atoms, clusters of metal atoms, metal ions and even metal surfaces interact with benzene and other aromatics [8–11]. While the structure, reactivity and thermochemistry of benzene, and the complexes it forms with metals, have been extensively investigated [12,13], much less consideration has been given to the biologically important nitrogen-containing heterocycles. In the literature, one can find threshold collision-induced dissociation studies and theoretical calculations of the metal-ion binding affinities of the nucleic bases [14], adenine [15], some of the azoles [16,17] and azines [18], pyridine [19] and substituted pyridines [20,21], and pyrimidine [22], but reactivity studies are essentially not available. Of interest in this study is the nitrogen heterocycle pyrrole (C_4H_5N). This five-member aromatic is important in a biological context because of its occurrence in porphyrins and proteins, however, relatively little is known about the reactivity and coordination geometry of pyrrole in organometallic complexes [23]. Robert Dunbar, Stephen Klippenstein and their group have recently investigated, by experiment and quantum chemistry, the interactions of pyrrole with a number of main-group and transition-metal cations [24]. They were able to show that pyrrole is somewhat unique among nitrogen heterocycles in that π-site bonding is preferred over N-site bonding in both the singly-ligated M^+(pyrrole) and doubly ligated M^+(pyrrole)$_2$ cations. Bakhtiar and Jacobson have studied the reactivity of Fe^+ and FeL^+ (L = O, C_4H_6, c-C_5H_6, C_5H_5, C_6H_6, C_5H_4(=CH_2)) with pyrrole [25].

Here, we begin the experimental investigation of the gas-phase reactivities of M^+(pyrrole)$_{1,2}$ cations towards simple gases that participate in biological activity. We focus on the reactivities of Ni^+(pyrrole)$_{1,2}$ and Cu^+(pyrrole)$_{1,2}$ cations towards CO and O_2. Also, we use quantum chemical calculations to analyze the structures and energetics of the resulting metal–pyrrole–ligand cations. Comparisons are made with measured reactivities of the atomic Ni^+ and Cu^+ cations and this establishes the influence of the binding with pyrrole on chemical reactivity. Ni^+ and Cu^+ were chosen for this study because both metal ions are important and ubiquitous in bioorganometallic systems. The study of gas-phase reactions eliminates effects of solvation, and so establishes intrinsic reactivities that can serve as a benchmark for the reactivities of bioorganometallic systems in vivo that involve the same metal bond connectivities.

2. Methods

2.1. Experimental

The kinetic and equilibrium measurements were taken with an inductively-coupled plasma/selected-ion flow tube (ICP-SIFT) tandem mass spectrometer. The SIFT apparatus and ICP ion source, as well as the ICP-SIFT interface, have been described previously [26–29]. Ni^+ and Cu^+ ions were generated in the ICP source, mass analyzed with a quadrupole mass filter and injected into the flow tube continuously flushed with helium buffer gas at 0.35 ± 0.01 Torr and 295 ± 2 K. At the operating temperature of the argon plasma estimated to be 5500 K, the Cu^+ is produced primarily (99%) in the ^{1}S ground electronic state whereas Ni^+ has the following distribution of electronic states: ^{2}D (81%), ^{4}F (16%) and ^{2}F (2%) [30]. Both atomic ions are produced largely in their ground electronic states and further relaxation into the ground state may proceed before the ions enter the reaction region of the flow tube. The helium buffer acts to thermalize the kinetic energy by collisions of the atomic ions with the He atoms.

Pyrrole vapor was introduced upstream in the flow tube through an inlet tube. Reactions of the Ni^+ and Cu^+ metal cations with pyrrole generate adducts, with up to two molecules of pyrrole clustering to the metal cation. The flow of pyrrole vapor was optimized to

maximize either the production of M^+(pyrrole) or of M^+(pyrrole)$_2$ downstream. The M^+(pyrrole)$_{1,2}$ ions are thermalized by collisions with the He buffer gas (about 10^5 collisions) before entering the second reaction region downstream in the flow tube where the neutral reagent molecules (CO, O_2) were added. The collisions with He ensure that the reactant ions reach a temperature prior to the reaction equal to the tube temperature of 295 ± 2 K.

Further downstream, a second quadrupole mass filter was used to monitor the intensities of reactant and product ions as a function of the flow of the neutral reagent. Rate coefficients for the primary reactions of all ions present in the system are determined with an uncertainty of ±30% from the rate of decay of the reactant ion intensity using pseudo-first-order kinetics. Higher-order rate coefficients are obtained by fitting the experimental data to the solutions of the system of differential equations for sequential reactions.

Pyrrole (Aldrich, 98%) was used without further purification. The neutral reagent molecules were introduced into the reaction region as a solution in helium (10–20%). The O_2 gas was of ultra-high purity grade (99.98%) and obtained from Liquid Carbonic Canada, Ltd. The CO gas was of C.P. grade (99.5%) and obtained from Canadian Liquid Air Ltd.

2.2. Theoretical

Theoretical calculations have been performed to determine structures and energies for some of the metal–pyrrole–ligand cationic complexes that were observed to be formed. Optimized structures, vibrational frequencies and rotational constants were computed using density functional theory (DFT) with the B3LYP (Becke-3 Lee–Yang–Parr) hybrid functional [31–34]. Vibrational frequencies were used both to characterize each stationary point found as a true minimum and to provide the thermochemical data (zero-point vibrational energies and thermal corrections) necessary for calculating binding energies.

The DZVP [35,36] basis-set was employed to accommodate and appropriately describe both nickel and copper. Both Holland and Castleman [37], and Shoeib et al. [38] have shown that energies obtained for Ag^+ bonded to H_2O, NH_3, organonitriles and pyridine using DZVP are in close agreement with experiment. Unless otherwise indicated, full counterpoise corrections for the basis-set superposition errors (BSSE) [39–41] are also included in the values reported for D_e, D_0, D_{298} and ΔG°_{298}; they were performed at the B3LYP/DZVP level of theory. All calculations were performed using Gaussian 98 software [42].

3. Results and discussion

Ni^+ and Cu^+ ions were generated using the ICP source and these were allowed to form pyrrole adducts upstream in the flow tube prior to reacting with the neutral reagent molecules CO and O_2 downstream. Up to two molecules of pyrrole were observed to attach to the metal cations, presumably by termolecular addition with helium buffer gas acting as a collisional stabilizing agent. Measured ion profiles for the atomic metal cations, as well as the pyrrole mono-adducts of Ni^+ and Cu^+ ions, reacting with O_2 are shown in Fig. 1. The equivalent ion profiles for reactions with CO are shown in Fig. 2.

Measured effective bimolecular rate coefficients for reactions with O_2 are shown in Table 1 while those with CO are shown in Table 2. The rate coefficients for primary reactions of pyrrole mono-adducts range from 2.6×10^{-13} to 1.6×10^{-10} cm^3 molecule^{-1} s^{-1} and are, in every case, equal to, or higher than the reaction rate coefficients for atomic metal cations which range

Table 1
Effective bimolecular rate coefficients, k_{obs}, measured for reactions of M^+, M^+(pyrrole) and M^+(pyrrole)$_2$ with O_2 in helium buffer gas at 0.35 ± 0.01 Torr and 295 ± 2 K

Reaction	k_{obs} (cm^3 molecule^{-1} s^{-1})
$Ni^+ + O_2$	2.0×10^{-13}
$Ni^+(O_2) + O_2$	1.5×10^{-11}
$Ni^+(O_2)_2 + O_2$	$<1.0 \times 10^{-13}$
Ni^+(pyrrole) + O_2	$\geq 4.6 \times 10^{-11}$
$Cu^+ + O_2$	2.4×10^{-13}
$Cu^+(O_2) + O_2$	1.7×10^{-12}
Cu^+(pyrrole) + O_2	$\geq 2.6 \times 10^{-13}$

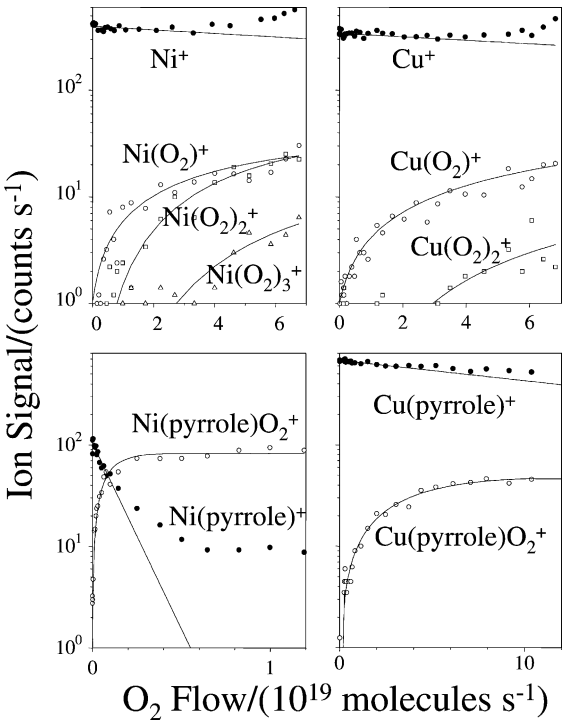

Fig. 1. Composite of ICP-SIFT results for the reactions of Ni^+, Cu^+, Ni^+(pyrrole) and Cu^+(pyrrole) with O_2 in helium buffer gas at 0.35 ± 0.01 Torr and 295 ± 2 K.

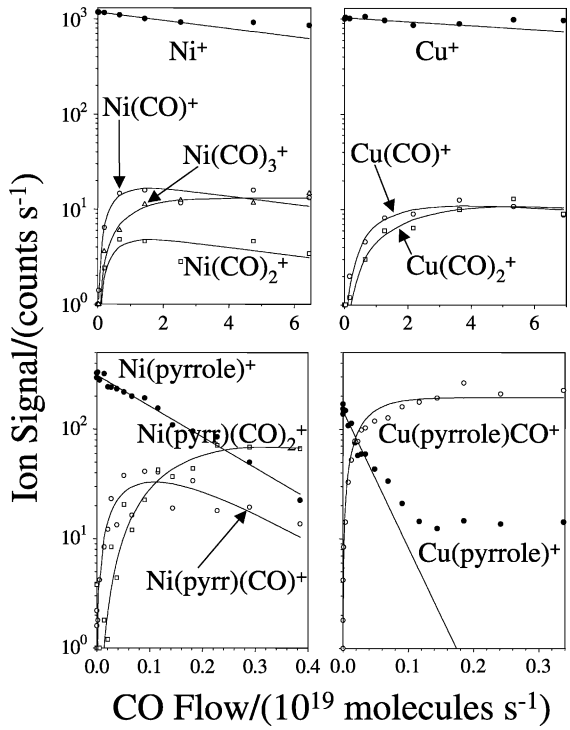

Fig. 2. Composite of ICP-SIFT results for the reactions of Ni^+, Cu^+, Ni^+(pyrrole) and Cu^+(pyrrole) with CO in helium buffer gas at 0.35 ± 0.01 Torr and 295 ± 2 K.

from 2.0×10^{-13} to 5.6×10^{-13} cm^3 $molecule^{-1}$ s^{-1}. The bis-adducts of both Ni^+ and Cu^+ were observed to add CO.

3.1. Reactions with O_2

3.1.1. Reactions of Ni^+ and Cu^+ with O_2

The atomic metal ions Ni^+ and Cu^+ were found to be only slightly reactive with molecular oxygen. In both cases, sequential addition of O_2 molecules was observed, as indicated in Eqs (1) and (2).

$$M^+ + O_2 + He \rightarrow MO_2^+ + He \quad (1)$$

$$M^+(O_2)_n + O_2 + He \rightarrow M^+(O_2)_{n+1} + He \quad (2)$$

Fig. 1 shows that up to three molecules of O_2 were observed to ligate to Ni^+, while up to two were observed to ligate to Cu^+. These reactions are assumed to be termolecular, facilitated by collisional stabilization with

Table 2
Effective bimolecular rate coefficients, k_{obs}, measured for reactions of M^+, M^+(pyrrole) and M^+(pyrrole)$_2$ with CO in helium buffer gas at 0.35 ± 0.01 Torr and 295 ± 2 K

Reaction	k_{obs} (cm^3 $molecule^{-1}$ s^{-1})	Reaction	k_{obs} (cm^3 $molecule^{-1}$ s^{-1})
$Ni^+ + CO$	5.6×10^{-13}	Ni^+(pyrrole) + CO	3.6×10^{-11}
$Ni^+(CO) + CO$	$<1.0 \times 10^{-13}$	Ni^+(pyrrole)CO + CO	$\geq 6.9 \times 10^{-11}$
$Ni^+(CO)_2 + CO$	$<1.0 \times 10^{-13}$	$Ni^+(pyrrole)_2 + CO$	$\geq 4.3 \times 10^{-12}$
$Cu^+ + CO$	2.8×10^{-13}	Cu^+(pyrrole) + CO	$\geq 1.6 \times 10^{-10}$
$Cu^+(CO) + CO$	$<1.0 \times 10^{-13}$	$Cu^+(pyrrole)_2 + CO$	observed

He atoms (the buffer gas). Rate coefficients have been determined for the first two additions of O_2. However, due to the very low ion intensity, a rate coefficient could not be accurately determined for the addition of a third molecule of O_2 to Ni^+. Rate coefficients for the primary O_2 addition reactions were measured to be 2.0×10^{-13} and 2.4×10^{-13} cm^3 molecule^{-1} s^{-1} for Ni^+ and Cu^+, respectively. The measured rate coefficients for the second addition of O_2 are more than 10 times larger that those reported for the first addition. This enhanced reactivity arises from the increased lifetime of the intermediate collision complex. The presence of the first molecule of O_2 substantially increases the degrees of freedom and therefore the lifetime of the collision complex involving the second O_2 molecule, thus allowing for more effective collisional stabilization. Bimolecular reactions involving the transfer of an electron, an O-atom or an oxide anion as indicated in Eqs. (3)–(5), respectively, were not observed.

$$M^+ + O_2 \rightarrow M + O_2^+ \quad (3)$$

$$M^+ + O_2 \rightarrow MO^+ + O \quad (4)$$

$$M^+ + O_2 \rightarrow MO + O^+ \quad (5)$$

For M = Ni, reactions (3) and (4) are endothermic by 102.4 and 70.7 kcal mol^{-1}, respectively, and reaction (5) is endothermic by 162–170 kcal mol^{-1}. For M = Cu, reactions (3) and (4) are endothermic by 100.0 and 86.6 kcal mol^{-1}, respectively, and reaction (5) is endothermic by 86–106 kcal mol^{-1}. Thermochemical data was obtained from the *Journal of Physical and Chemical Reference Data* [43] and the *NIST Chemistry Web Book* [44].

3.1.2. Reactions of Ni^+(pyrrole) and Cu^+(pyrrole) with O_2

Both Ni^+(pyrrole) and Cu^+(pyrrole) were observed to be reactive with O_2. Fig. 1 shows that each of these ions ligates only one molecule of O_2 under our experimental conditions. Once again, the ligated ions are assumed to be stabilized by collisions with atoms of He. No bimolecular reactions, including the ligand-switching reaction (6), were observed, presumably because they are endothermic.

$$M^+(\text{pyrrole}) + O_2 \rightarrow MO_2^+ + \text{pyrrole} \quad (6)$$

Failure to observe the occurrence of reaction (6) implies that O_2 ligates less strongly to the metal ions Ni^+ and Cu^+ than pyrrole and that $D(M^+–O_2) < D(M^+–\text{pyrrole})$, where M = Ni, Cu.

Equilibrium analyses of the kinetic data involving a plot of $[M^+(\text{pyrrole})(O_2)]/[M^+(\text{pyrrole})]$ vs. O_2 flow provided lower limits for K_{eq}. We obtained values of $K_{eq} \geq 9.7 \times 10^6$ and $\geq 1.0 \times 10^4$ for the reactions of Ni^+(pyrrole) and Cu^+(pyrrole), respectively. These provide lower limits for $-\Delta G^\circ$ of 9.4 and 5.4 kcal mol^{-1} for the respective reactions of Ni^+(pyrrole) and Cu^+(pyrrole).

3.1.3. Reactions of $Ni^+(pyrrole)_2$ and $Cu^+(pyrrole)_2$ with O_2

The bis-pyrrole adducts of both Ni^+ and Cu^+ were observed to be unreactive with O_2 with $k < 10^{-13}$ cm^3 molecules^{-1} s^{-1}. As with the reactions of M^+(pyrrole) with O_2, no ligand-switching reactions were observed, suggesting that $D(M^+(\text{pyrrole})–O_2) < D(M^+(\text{pyrrole})–\text{pyrrole})$, where M = Ni, Cu or that the activation barrier to switching is high for the bis-sandwich metal which is protected from O_2 penetration.

3.2. Reactions with CO

3.2.1. Reactions of Ni^+ and Cu^+ with CO

As with the reactions of the atomic metal ions with O_2, only sequential termolecular addition of CO was observed, as is shown in Fig. 2. The observed ligation of CO molecules to Ni^+ and Cu^+ perfectly mirrored the O_2 reactions: up to three molecules were observed to ligate to Ni^+, while up to two were observed to ligate to Cu^+ under our experimental conditions. Rate coefficients could be determined only for the first addition of CO. They were measured to be 5.6×10^{-13} and 2.8×10^{-13} cm^3 molecule^{-1} s^{-1} for Ni^+ and Cu^+, respectively.

Again, as was the case for the reactions with O_2, no bimolecular products were formed. Thermochem-

ical data indicates that for reactions of Ni^+ with CO the transfer of an O-atom would be endothermic by 208.8 kcal mol^{-1}, while the transfer of an electron would be endothermic by 87 kcal mol^{-1}. Similarly, the transfer of an O-atom or an electron from CO to Cu^+ would be endothermic by 224.7 and 84.6 kcal mol^{-1}, respectively. Thermochemical data was obtained from the *Journal of Physical and Chemical Reference Data* [43] and the *NIST Chemistry Web Book* [44].

3.2.2. Reactions of Ni^+(pyrrole) and Cu^+(pyrrole) with CO

Fig. 2 shows that both Ni^+(pyrrole) and Cu^+(pyrrole) add CO under our experimental conditions, but Cu^+(pyrrole) does so about four times faster. Only Ni^+(pyrrole) was observed to add a second CO molecule with $k \geq 6.9 \times 10^{-11}$ cm^3 molecule^{-1} s^{-1}. No bimolecular products were observed. Failure to observe ligand switching as a primary reaction implies that CO ligates less strongly to the metal ions Ni^+ and Cu^+ than pyrrole and that $D(M^+–CO) < D(M^+–pyrrole)$, where M = Ni, Cu.

The addition of CO to Cu^+(pyrrole) was observed to approach equilibrium while the addition of CO to Ni^+(pyrrole)(CO) actually achieved equilibrium. We obtain values of $K_{eq} \geq 7.9 \times 10^7$ ($\Delta G^\circ \leq -10.6$ kcal mol^{-1}) and $K_{eq} = 9.3 \times 10^6$ ($\Delta G^\circ = -9.3$ kcal mol^{-1}) for the reactions of Cu^+(pyrrole) and Ni^+(pyrrole)(CO), respectively.

3.2.3. Reactions of $Ni^+(pyrrole)_2$ and $Cu^+(pyrrole)_2$ with CO

Addition of a single molecule of CO was the only reaction observed with $Ni^+(pyrrole)_2$ and an effective bimolecular rate coefficient of $k \geq 4.3 \times 10^{-12}$ cm^3 molecule^{-1} s^{-1} was measured for this reaction. The addition was observed to approach equilibrium with $K_{eq} \geq 4.3 \times 10^5$ ($\Delta G^\circ \leq -7.6$ kcal mol^{-1}). $Cu^+(pyrrole)_2$ appeared to be much less reactive and only small amounts of the CO adduct were observed to be formed. The failure to observe a ligand-switching reaction suggests that CO binds less strongly to Ni^+(pyrrole) and Cu^+(pyrrole) than does pyrrole itself, viz. $D(Ni^+(pyrrole)–CO) < D(Ni^+(pyrrole)–pyrrole)$ and $D(Cu^+(pyrrole)–CO) < D(Cu^+(pyrrole)–pyrrole)$, or that the activation barrier to switching is high for the bis-sandwich metal which is protected from CO penetration.

3.3. Variation in the rate of ligation with the number of pyrrole ligands

Our experimental measurements indicate a strong dependence of the reaction rate coefficient upon the number of pyrrole ligands attached to the transition-metal ion even though only lower limits were measurable in all but one case (Ni^+(pyrrole) + CO) due to the approach to, and attainment of, equilibrium. For the most part, the rate coefficients for the ligation of pyrrole mono-adducts are at least 50 times higher than those for the ligation of the atomic metal cations. This can be accounted for by an increase in the lifetime of the intermediate collision complex due primarily to an increase in the number of degrees of freedom provided by the pyrrole ligand for the intramolecular redistribution of excess energy. The ligation of Cu^+ with O_2 is an apparent exception in that the rate coefficient for ligation appears to be insensitive to the presence of pyrrole. In this case, however, equilibrium is achieved quickly so that the initial decay of Cu^+(pyrrole) provides a low lower limit for the apparent bimolecular rate coefficient.

The pyrrole bis-adducts of Ni^+ and Cu^+ were observed to be reactive only with the CO ligand (see Table 2).

3.4. Variation in the ligation of the atomic metal ions (Ni^+, Cu^+)

In general, the experimental results indicate that Cu^+ ($^1S_0$, $3d^{10}$) binds two molecules of O_2 and CO while Ni^+ ($^2D_{5/2}$, $3d^9$) binds three.

3.5. Theoretical structures and energies

Theoretical calculations have been performed to determine structures and energies of the atomic Ni^+ and Cu^+ ions ligated with O_2 and CO and for some

Table 3
Calculated theoretical bond dissociation energies for M^+–CO and (OC)M^+–CO

Species	D_e (kcal mol^{-1})[a]	D_e (kcal mol^{-1})[b]	D_{298} (kcal mol^{-1})[c]	D_{298} (kcal mol^{-1})[d]
Ni^+–CO	44.2	36.7	38.0	42.4
(OC)Ni^+–CO	41.0	34.7	32.7	40.4
Cu^+–CO	42.5	33.4	35.8	35.5[e]
(OC)Cu^+–CO	41.1	35.5	32.6	41.0[e]

[a] This work, not corrected for BSSE.
[b] Theory [35], not corrected for BSSE.
[c] This work, corrected for BSSE.
[d] Experimental results from Armentrout and co-workers [46,47].
[e] Reported values for D_0.

of the metal–pyrrole and metal–pyrrole–ligand complexes that were observed experimentally. Our results for the bare metal ions can be compared with results of ab initio calculations reported by Barnes et al. [45] for transition-metal mono- and di-carbonyl cations including those for Ni and Cu. Gapeev et al. [24] have reported density functional calculations using the B3LYP hybrid functional for pyrrole adducts of metal cations including those for Ni and Cu.

Table 3 compares bond dissociation energies for Cu^+–CO, Ni^+–CO, Cu^+(CO)–CO, Ni^+(CO)–CO computed by us and Barnes et al. [45]. Our values for D_e are systematically higher by up to as much as 10 kcal mol^{-1} and more in line with the experimental values compiled by Barnes et al. [45] and reported by Armentrout and co-workers [46,47]. There is good agreement in the computed bond lengths that are shown in Fig. 3. We also calculated

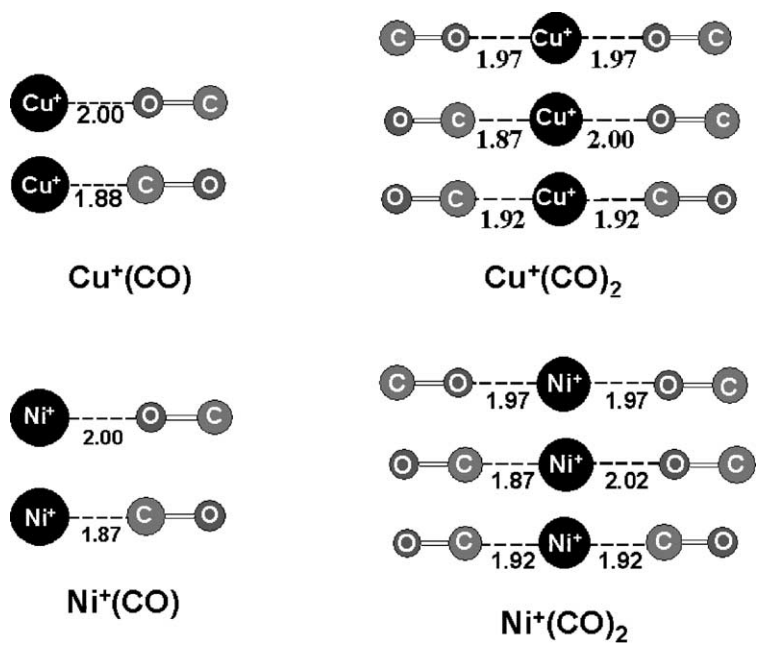

Fig. 3. Computed structures and bond lengths (in Å) for M^+–C and M^+–O bonded isomers of M^+(CO) and $M^+(CO)_2$ with M = Ni and Cu.

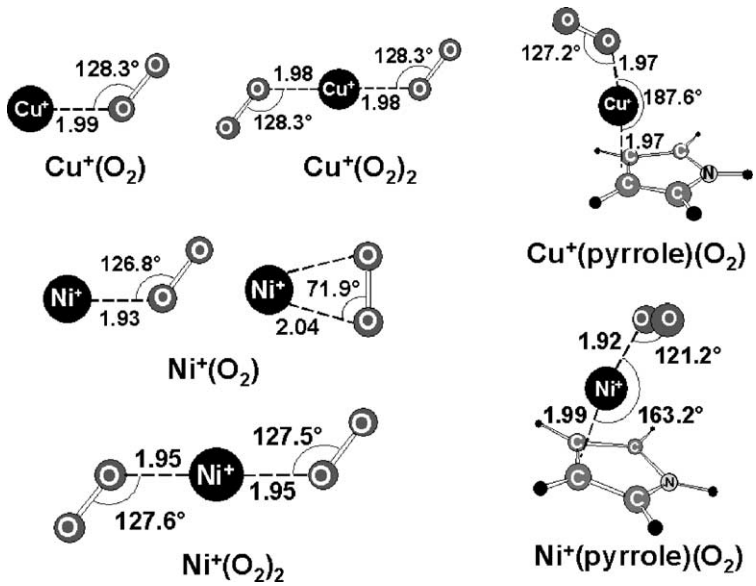

Fig. 4. Computed structures and bond lengths (in Å) for $M^+(O_2)$, $M^+(O_2)_2$ and M^+(pyrrole)(O_2) with M = Ni and Cu.

M^+–O bonded isomers of Cu^+–CO, Ni^+–CO, Cu^+(CO)–CO, Ni^+(CO)–CO and these are shown in Fig. 3 as well. Our calculations indicate that M^+–C interaction is thermodynamically favored over M^+–O interaction in every case studied, which is consistent with a primarily electrostatic interaction between the positively charged metal and the partial negative charge on the carbon in CO. Fig. 4 includes computed structures for $Cu^+(O_2)_{1,2}$ and $Ni^+(O_2)_{1,2}$. We are not aware of previous calculations for these species. The structures obtained for the various metal ion–CO complexes were all found to be linear, as can be seen in Fig. 3. However, the metal ion–O_2 complexes were found to have bent structures. The bond angles for the metal ion–O_2 structures range from 126.8 to 128.3°, as denoted in Fig. 4. The CO molecule can be considered to be sp-hybridized, and thus the lone pair that participates in ligation lies along the internuclear axis, resulting in a linear metal ion–CO structure. The O_2 molecule is more complicated. We think of the half-filled p_z orbitals as forming a sigma bond along the internuclear axis, while one half-filled and one filled p-orbital from each O atom combine to form a π-orbital. There is thus a depletion of electron density along the bond axis behind each O atom and, as a result, the linear metal–O_2 structure is highly unlikely. Rather, the metal ion will interact with the π-orbital, preferring to sit closer to one or the other of the O atoms where the electron density is the highest. Upon interacting with the O_2 molecule, the metal ion will give up some of its positive charge, most of which will reside on the farther O atom to achieve a maximum separation of charge. It then follows that the metal must experience a slight repulsion causing it to lean away from the farther O-atom. This would account for the type of bent metal ion–O_2 structures depicted in Fig. 4.

Table 4 compares the theoretical results obtained in this study for Ni^+–pyrrole and Cu^+–pyrrole with those reported by Gapeev et al. [24]. Both binding energies (D_0) and the geometrical parameters of interest, namely, the metal–pyrrole bond length ($R_{M\text{-ring}}$) and the offset distance of the metal from the edge of the pyrrole ring (Δx), are included in Table 4. The geometrical parameters are defined in Graphic 1. As did Gapeev et al., we conclude from our computations that both metal ions prefer to bind to the π-system of the pyrrole ring and not to the nitrogen

Table 4
Computed theoretical distance parameters (see Graphic 1) and binding energies for M^+(pyrrole) and M^+(pyrrole)$_2$

Species	$R_{M\text{-ring}}$ (Å)[a]	Δx (Å)[b]	D_0 (kcal mol^{-1})[c]	Gapeev et al. [24]		
				$R_{M\text{-ring}}$ (Å)[a]	Δx (Å)[b]	D_0 (kcal mol^{-1})[c]
Ni^+–pyrrole	1.98	0.00	59.5	1.98	0.15	61.0
Cu^+–pyrrole	1.98	−0.16	61.0	1.99	−0.33	58.3
Ni^+(pyrrole)$_2$	2.03	0.08	42.5	1.98	−0.06	43.7
Cu^+(pyrrole)$_2$	2.03	−0.22	37.4	1.95	−0.37	38.7

[a] $R_{M\text{-ring}}$, distance from metal ion to the CCCC plane.
[b] Δx, offset distance from the edge of the pyrrole ring (negative values are outside of the pyrrole ring).
[c] D_0, BSSE-corrected binding energy.

atom core. Binding at the nitrogen atom is inhibited by the accumulation of positive charge that results in strong electrostatic repulsion. Our calculated values of D_0 are in good agreement with those obtained by Gapeev et al. [24]. The $R_{M\text{-ring}}$ values are also in good agreement, with our values for the pyrrole bis-adducts being slightly higher. The largest differences between the two sets of calculations are in the Δx values, in particular, for the Ni^+-containing structures. Gapeev et al. place the Ni^+ ion within the perimeter of the pyrrole ring by 0.15 Å for the Ni^+(pyrrole) structure while our calculations indicate that the metal lies immediately above the C–C bond opposite the nitrogen. The situation is reversed when we compare the values obtained for the Ni^+(pyrrole)$_2$ structure. Our calculations indicate that the Ni^+ ion lies 0.08 Å inside the perimeter of the ring whereas Gapeev et al. place the metal ion 0.06 Å outside.

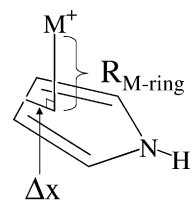

Graphic 1

For metal–pyrrole–ligand structures, we have found that an additional parameter must be considered, namely, the offset of the metal from the midline of the pyrrole ring (Δy). This additional parameter is defined in Graphic 2. Table 5 lists the three computed geometrical parameters of interest ($R_{M\text{-ring}}$, Δx, Δy) for every metal–pyrrole–ligand structure that was calculated in this study. To our knowledge, there are no literature values available for comparison. The values of Δy in Table 5 indicate that the addition of a CO

Table 5
Computed theoretical distance parameters (see Graphic 2) and binding energies for M^+(pyrrole)L and M^+(pyrrole)$_2$L

Structure	$R_{M\text{-ring}}$ (Å)[a]	Δx (Å)[b]	Δy (Å)[c]
Ni^+(pyrrole)CO	2.02	0.17	0.21
Ni^+(pyrrole)OC	1.98	0.16	0.41
Ni^+(pyrrole)(CO)$_2$	2.10	0.04	0.00
Ni^+(pyrrole)(OC)$_2$	2.03	0.04	−0.37
Ni^+(pyrrole)(CO)(OC)	2.27	0.05	−0.20
Ni^+(pyrrole)$_2$CO	2.08, 2.15	0.29, 0.19	1.45, −0.84
Ni^+(pyrrole)O_2	2.00	0.09	−0.06
Cu^+(pyrrole)O_2	1.98	−0.31	0.01
Cu^+(pyrrole)CO	2.03	−0.18	−0.04
Cu^+(pyrrole)OC	1.97	−0.32	−0.04

[a] $R_{M\text{-ring}}$, distance from metal ion to the CCCC plane.
[b] Δx, offset distance from the edge of the pyrrole ring (negative values are outside of the pyrrole ring).
[c] Δy, offset distance of the metal ion from the midline of pyrrole (positive values indicate offset to the right).

ligand can skew the symmetry inherent in M^+–pyrrole complexes by shifting the position of the metal ion relative to the midline of the pyrrole molecule. Interestingly, the addition of a second CO ligand restores the symmetry in the case of Ni^+–C bonding but not Ni^+–O bonding. Addition of an O_2 ligand does not significantly shift the metal from the midline of the pyrrole molecule. Computed theoretical structures, bond lengths and angles for the Ni^+(pyrrole)(O_2) and Cu^+(pyrrole)(O_2) are given in Fig. 4 while those for Ni^+(pyrrole)(CO), Cu^+(pyrrole)(CO), Ni^+(pyrrole)$(CO)_2$ and Ni^+(pyrrole)$_2$(CO) are given in Fig. 5.

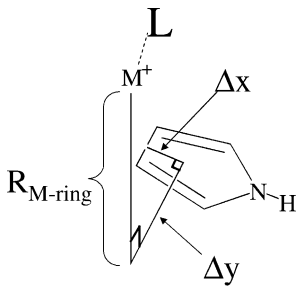

Graphic 2

For structures containing CO, both metal–C and metal–O binding was considered. Our calculations indicate that in every instance metal–C binding is thermodynamically favored over metal–O bonding. The metal–C vs. metal–O binding effect is around 20 kcal mol^{-1} with some exceptions (see Table 7). For the addition of the first CO ligand to either the bare metal or the pyrrole adduct the effect is always 23 ± 1 kcal mol^{-1}. For the addition of the second CO ligand to either the bare metal or the pyrrole adduct, the effect is only slightly reduced by up to 3 kcal mol^{-1} when the first ligand is metal–O bonded. This effect is reduced still further, to as low as 11 kcal mol^{-1}, when the first ligand is metal–C bonded.

Tables 6 and 7 list the computed values of ΔG°_{298} that were determined for the formation of the metal–pyrrole–O_2 and metal–pyrrole–CO adduct ions studied in this investigation. We note that ΔG°_{298} for the binding of pyrrole to either Ni^+ or Cu^+ is much more negative than for the binding of either O_2 or CO. This agrees with our experimental observation of the failure of any ligand-switching reactions involving the

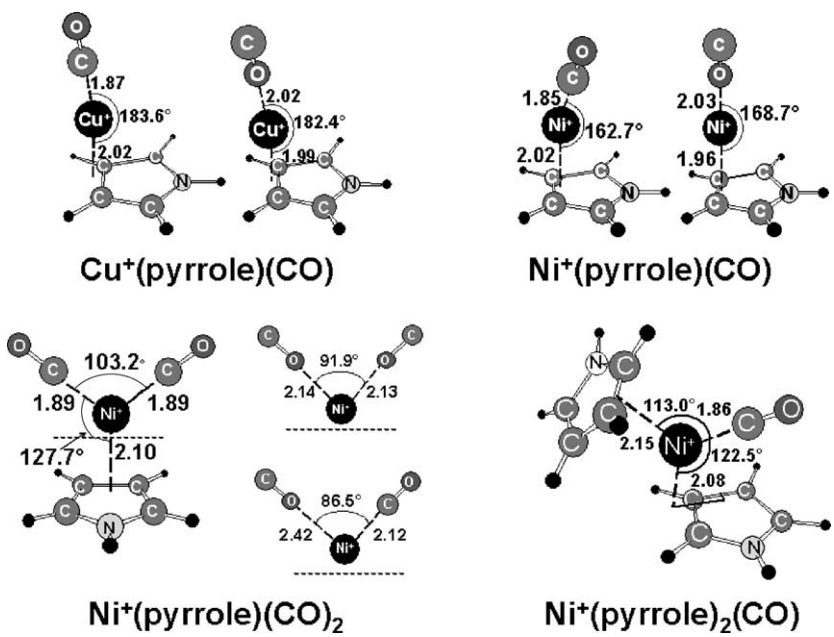

Fig. 5. Computed structures and bond lengths (in Å) for M^+(pyrrole)(CO) with M = Ni and Cu, M^+(CO) and $M^+(CO)_2$ with M = Ni and Cu, of Ni^+–C and Ni^+–O bonded isomers of Ni^+(pyrrole)$(CO)_2$ and of Ni^+(pyrrole)$_2$(CO).

Table 6
Computed theoretical ΔG°_{298} and D_e values[a] for ligation with O_2

Species	ΔG°_{298} (kcal mol^{-1})	D_e (kcal mol^{-1})[b]	Species	ΔG°_{298} (kcal mol^{-1})	D_e (kcal mol^{-1})[b]
Ni^+	–	–	Cu^+	–	–
Ni^+–O_2	−9.62	−16.64 (2.88)	Cu^+–O_2	−7.00	−13.85 (3.67)
O_2–Ni^+–O_2	−6.73	−14.21 (5.15)	O_2–Cu^+–O_2	−6.16	−14.37 (4.08)
Ni^+–O_2 (side)	−5.40	−11.91 (2.99)			
Ni^+	–	–	Cu^+	–	–
Ni^+–pyrrole	−51.96	−62.39 (5.20)	Cu^+–pyrrole	−53.17	−63.44 (2.82)
(Pyrrole)Ni^+–O_2	−3.17	−13.51 (3.81)	(Pyrrole)Cu^+–O_2	−0.81	−12.20 (2.70)
O_2–(pyrrole)Ni^+–O_2	+8.60	−0.27 (4.27)			
Ni^+	–	–	Cu^+	–	–
Ni^+–py	−51.96	–62.39 (5.20)	Cu^+–pyrrole	−53.17	−63.44 (2.82)
(Pyrrole)Ni^+–pyrrole	−31.96	−46.65 (2.98)	(Pyrrole)Cu^+–pyrrole	−28.39	−40.61 (6.74)
			(Pyrrole)$_2$-Cu^+–O_2	+11.47	+1.76 (2.24)

[a] Values of D_e and ΔG°_{298} have been corrected for BSSE.
[b] Values in parentheses denote the magnitude of the BSSE correction.

pyrrole ligand. Second, we note that the ligation of pyrrole slightly decreases (in absolute magnitude) the free energy of the ligation of O_2 or CO (with metal–C bonding) to the metal ions by up to 6 kcal mol^{-1}.

Except for the ligation of Ni^+(pyrrole)(CO) with CO, our experimental results provide only lower limits to the absolute values of ΔG°_{298}. As such, there is no close agreement between the limiting

Table 7
Computed theoretical ΔG°_{298} and D_e values[a] for ligation with CO

Species	ΔG°_{298} (kcal mol^{-1})	D_e (kcal mol^{-1})[b]	Species	ΔG°_{298} (kcal mol^{-1})	D_e (kcal mol^{-1})[b]
Ni^+	–	–	Cu^+	–	–
Ni^+–CO	−27.67	−40.70 (3.50)	Cu^+–CO	−28.22	−39.58 (2.98)
Ni^+(CO)–CO	−23.33	−37.17 (3.87)	Cu^+(CO)–CO	−22.52	−36.05 (5.06)
Ni^+(CO)–OC	−6.31	−18.71 (2.37)	Cu^+(CO)–OC	−6.01	−17.64 (3.82)
Ni^+–OC	−6.93	−17.83 (3.31)	Cu^+–OC	−8.01	−17.00 (3.00)
Ni^+(OC)–OC	−7.66	−18.31 (2.22)	Cu^+(OC)–OC	−0.48	−16.92 (4.28)
Ni^+(OC)–CO	−27.71	−41.40 (2.74)	Cu^+(OC)–CO	−26.11	−39.66 (4.36)
Ni^+	–	–	Cu^+	–	–
Ni^+–pyrrole	−51.96	−62.39 (5.20)	Cu^+–pyrrole	−53.17	−63.44 (2.82)
(Pyrrole)Ni^+–CO	−25.54	−36.70 (3.33)	(Pyrrole)Cu^+–CO	−22.62	−35.95 (2.76)
(Pyrrole)Ni^+(CO)–CO	−7.88	−19.91 (2.40)	(Pyrrole)Cu^+(CO)–CO	+0.99	−11.35 (3.52)
(Pyrrole)Ni^+(CO)–OC	+6.07	−3.56 (1.79)	(Pyrrole)Cu^+(CO)–OC	+2.82	−0.68 (1.39)
(Pyrrole)Ni^+–OC	−1.03	−12.57 (3.34)	(Pyrrole)Cu^+–OC	−2.52	−12.80 (3.10)
(Pyrrole)Ni^+(OC)–OC	+6.71	−3.92 (2.56)	(Pyrrole)Cu^+(OC)–OC	+4.67	−2.22 (1.45)
(Pyrrole)Ni^+(OC)–CO	−15.14	−26.12 (3.35)	(Pyrrole)Cu^+(OC)–CO	−11.52	−22.30 (2.58)
Ni^+	–	–	Cu^+	–	–
Ni^+–pyrolle	−51.96	−62.39 (5.20)	Cu^+–pyrrole	−53.17	−63.44 (2.82)
(Pyrrole)Ni^+–pyrrole	−31.69	−46.65 (2.98)	(Pyrrole)Cu^+–pyrrole	−28.39	−41.06 (6.29)
(Pyrrole)$_2$–Ni^+–CO	−0.25	−13.23 (3.32)			

[a] Values of D_e and ΔG°_{298} have been corrected for BSSE.
[b] Values in parentheses denote the magnitude of the BSSE correction.

experimental and the absolute theoretical values of ΔG°_{298}, although there is some semblance of agreement between the relative values. The measured value of $\Delta G^{\circ}_{298} = -9.3\,\text{kcal mol}^{-1}$ obtained for the ligation of Ni^+(pyrrole)(CO) with CO is most consistent with the computed value of $-7.88\,\text{kcal mol}^{-1}$ which corresponds to sequential addition of CO by metal–C bonding. The addition of CO by Ni^+–O bonding to Ni^+(pyrrole)(CO) is computed to be endoergic by $6.71\,\text{kcal mol}^{-1}$. Ni^+–O bonding of CO to Ni^+(pyrrole) itself is almost ergoneutral so that, if formed, Ni^+(pyrrole)(OC) is not likely to survive to add a second CO molecule by Ni^+–C bonding which is exoergic by $15.14\,\text{kcal mol}^{-1}$ according to the calculations. The analogous ligation of Cu^+(pyrrole)(CO) with CO by metal–C or metal–O bonding is computed to be endoergic and, indeed, was not observed in our experiments. The ligation of Ni^+(pyrrole)O_2 with another molecule of O_2 also is computed to be endoergic and also was not observed experimentally.

4. Conclusions

We have shown experimentally that M^+ and M^+(pyrrole) with M = Ni and Cu will ligate the diatomic ligands O_2 and CO and that bis-adduct ions will ligate CO at room temperature in helium buffer gas at 0.35 Torr. While atomic Cu^+ was observed to bind up to two ligands of O_2 and CO, atomic Ni^+ was observed to bind up to three. The presence of one molecule of pyrrole dramatically increases the gas-phase rate of metal-ion ligation. While equilibrium was observed to be approached in several of the ligation reactions, an absolute value for the standard free energy of ligation could be obtained only for the ligation of Ni^+(pyrrole)(CO) with CO. Comparisons with computed standard free energies of ligation in this case suggest the occurrence of the sequential ligation of two CO molecules to Ni^+(pyrrole) by Ni^+–C and not Ni^+–O bonding.

From our quantum chemical calculations, we can conclude that metal ion–CO complexes have a linear M–CO geometry, while structures of metal ion–O_2 complexes a bent M–O_2 geometry. The addition of a ligand of O_2 or CO can skew the symmetry inherent in M^+–pyrrole complexes (less so with O_2) by shifting the position of the metal ion relative to the midline of the pyrrole molecule. In the ligation with CO, metal–C bonding is always thermodynamically favored over metal–O bonding. The reaction free energy for the binding of pyrrole to either Ni^+ or Cu^+ is much more negative than for the binding of either O_2 or CO. This agrees with our failure experimentally to observe any ligand-switching reactions involving the pyrrole ligand. Also, the computations show that the ligation of pyrrole only slightly decreases the ligation energy of O_2 and CO to these metal ions.

Acknowledgements

Continued financial support from the Natural Sciences and Engineering Research Council of Canada is greatly appreciated. Also, we acknowledge support from the National Research Council, the Natural Science and Engineering Research Council and MDS SCIEX in the form of a Research Partnership grant. As holder of a Canada Research Chair in Physical Chemistry, Diethard K. Bohme thanks the contributions of the Canada Research Chair Program to this research.

References

[1] F.D. Lewis, J. Yang, C.L. Stern, J. Am. Chem. Soc. 118 (1996) 2772.
[2] A.V. Muehldorf, D.V. Engen, J.C. Warner, J. Am. Chem. Soc. 110 (1988) 6561.
[3] W.L. Jorgensen, D.L. Severance, J. Am. Chem. Soc. 112 (1990) 4768.
[4] R. Laatikainen, J. Ratilainen, R. Sebastian, H. Santa, J. Am. Chem. Soc. 117 (1995) 11006.
[5] J.C. Ma, D.A. Dougherty, Chem. Rev. 97 (1997) 1303.
[6] D.A. Dougherty, Science 271 (1996) 163.
[7] N.S. Scrutton, A.R.C. Raine, Biochem. J. 319 (1996) 1.
[8] P.L. Timms, Chem. Educ. 49 (1972) 782.
[9] W.E. Silverthorn, Adv. Organomet. Chem. 13 (1975) 47.
[10] D. Braga, P.J. Dyson, F. Grepioni, B.F.G. Johnson, Chem. Rev. 94 (1994) 1457.
[11] C.M. Friend, E.L. Muetterties, J. Am. Chem. Soc. 103 (1981) 773.

[12] E.L. Muetterties, J.R. Bleeke, E.J. Wucherer, T.A. Albright, Chem. Rev. 82 (1982) 499.
[13] F. Meyer, F.A. Khan, P.B. Armentrout, J. Am. Chem. Soc. 117 (1995) 9740.
[14] M.T. Rodgers, P.B. Armentrout, J. Am. Chem. Soc. 122 (2000) 8548.
[15] M.T. Rodgers, P.B. Armentrout, J. Am. Chem. Soc. 124 (2002) 2678.
[16] M.T. Rodgers, P.B. Armentrout, Int. J. Mass Spectrom. 185–187 (1999) 359.
[17] H. Huang, M.T. Rodgers, J. Phys. Chem. A 106 (2002) 4277.
[18] R. Amunugama, M.T. Rodgers, Int. J. Mass Spectrom. 195/196 (2000) 439.
[19] J.R. Stanley, R. Amunugama, M.T. Rodgers, J. Am. Chem. Soc. 122 (2000) 10969.
[20] M.T. Rodgers, J. Phys. Chem. A 105 (2001) 2374.
[21] M.T. Rodgers, J. Phys. Chem. A 105 (2001) 8145.
[22] R. Amunugama, M.T. Rodgers, J. Phys. Chem. A 105 (2001) 9883.
[23] D.L. Kershner, F. Basolo, J. Am. Chem. Soc. 109 (1987) 7396.
[24] A. Gapeev, C. Yang, S.J. Klippenstein, R.C. Dunbar, J. Phys. Chem. A 104 (2000) 3246.
[25] R. Bakhtiar, D.B. Jacobson, J. Am. Soc. Mass Spectrom. 7 (1996) 938.
[26] G.I. Mackay, G.D. Vlachos, D.K. Bohme, H.I. Schiff, Int. J. Mass Spectrom. Ion Phys. 36 (1980) 259.
[27] A.B. Raksit, D.K. Bohme, Int. J. Mass Spectrom. Ion Processes 55 (1983/84) 69.
[28] G.K. Koyanagi, V. Lavrov, V.I. Baranov, D. Bandura, S.D. Tanner, J.W. McLaren, D.K. Bohme, Int. J. Mass Spectrom. Ion Processes 194 (2000) L1.
[29] G.K. Koyanagi, V.I. Baranov, S.D. Tanner, D.K. Bohme, J. Anal. At. Spectrom. 15 (2000) 1207.
[30] G.K. Koyanagi, D. Caraiman, V. Blagojevic, D.K. Bohme, J. Phys. Chem. A 108 (2002) 4581.
[31] A.D. Becke, J. Chem. Phys. 96 (1992) 2155.
[32] A.D. Becke, J. Chem. Phys. 98 (1993) 5648.
[33] C. Lee, W. Yang, R.G. Parr, Phys. Rev. B 37 (1998) 785.
[34] P.J. Stephens, F.J. Devlin, C.F. Chablowski, M. Frisch, J. Phys. Chem. 98 (1994) 11623.
[35] N. Godbout, D.R. Salahub, J. Andzelm, E. Wimmer, Can. J. Chem. 70 (1992) 560.
[36] N. Godbout, Ensemble de base pour la theorie de la fonctionnelle de la densite-structures moleculaires, proprietes mono-electroniques et modeles de zeolites, PhD Thesis, Department of Chemistry, University of Montreal, 1996.
[37] P.M. Holland, A.W. Castleman Jr., J. Chem. Phys. 76 (1982) 4195.
[38] T. Shoeib, H. El Aribi, K.W.M. Siu, A.C. Hopkinson, J. Phys. Chem. 105 (2001) 710.
[39] S.F. Boys, F. Bernardi, Mol. Phys. 19 (1970) 553.
[40] G. Chalasinski, M.M Szczesniak, Chem. Rev. 94 (1994) 1723.
[41] F.B. van Duijneveldt, JGCM van Duijneveldt-van de Rijdt, J.H van Lenthe, Chem. Rev. 94 (1994) 1873.
[42] M.J. Frisch, G.W. Trucks, H.B. Schlegel, G.E. Scuseria, M.A. Robb, J.R. Cheeseman, V.G. Zakrzewski, J.A. Montgomery, R.E. Stratmann, J.C. Burant, S. Dapprich, J.M. Millam, A.D. Daniels, K.N. Kudin, M.C. Strain, O. Farkas, J. Tomasi, V. Barone, M. Cossi, R. Cammi, B. Mennucci, C. Pomelli, C. Adamo, S. Clifford, J. Ochterski, G.A. Petersson, P.Y. Ayala, Q. Cui, K. Morokuma, D.K. Malick, A.D. Rabuck, K. Raghavachari, J.B. Foresman, J. Cioslowski, J.V. Ortiz, B.B. Stefanov, G. Liu, A. Liashenko, P. Piskorz, I. Komaromi, R. Gomperts, R.L. Martin, D.J. Fox, T. Keith, M.A. Al-Laham, C.Y. Peng, A. Nanayakkara, C. Gonzalez, M. Challacombe, P.M.W. Gill, B.G. Johnson, W. Chen, M.W. Wong, J.L. Andres, M. Head-Gordon, E.S. Replogle, J.A. Pople, Gaussian 98 (Revision A.7), Gaussian, Inc., Pittsburgh, PA, 1998.
[43] S.G. Lias, J.E. Bartmess, J.F. Liebman, J.L. Holmes, R.D. Levin, W.G. Mallard, Journal of Physical and Chemical Reference Data “Gas-Phase Ion and Neutral Thermochemistry”, vol. 8, suppl. 1, American Chemical Society and American Institute of Physics, 1988.
[44] NIST Chemistry Web Book, NIST Standard Reference Database, http://webbook.nist.gov/chemistry/.
[45] L.A. Barnes, M. Rozi, C.W. Bauschlicher Jr., J. Chem. Phys. 93 (1990) 609.
[46] F. Meyer, Y.-M. Chen, P.B. Armentrout, J. Am. Chem. Soc. 117 (1995) 4071.
[47] F.A. Khan, D.L. Steele, P.B. Armentrout, J. Phys. Chem. 99 (1998) 7819.